analytical chemistry

ARTICLE

pubs.acs.org/ac

Improving Peak Capacity in Fast Online Comprehensive Two-Dimensional Liquid Chromatography with Post-First-Dimension Flow Splitting

Marcelo R. Filgueira,[†,‡] Yuan Huang,[†] Klaus Witt,[§] Cecilia Castells,[‡] and Peter W. Carr*[,†]

[†]Department of Chemistry, Smith and Kolthoff Halls, University of Minnesota, 207 Pleasant St. S.E., Minneapolis, Minnesota 55455, United States

[‡]Div Quim Analit, Fac Ciencias Exactas, Univ Nacl La Plata, 47 y 115, La Plata RA-1900, Argentina

[§]Agilent Technologies Germany GmbH, Hewlett−Packard Str. 8, Waldbronn, BW 76337, Germany

ABSTRACT:

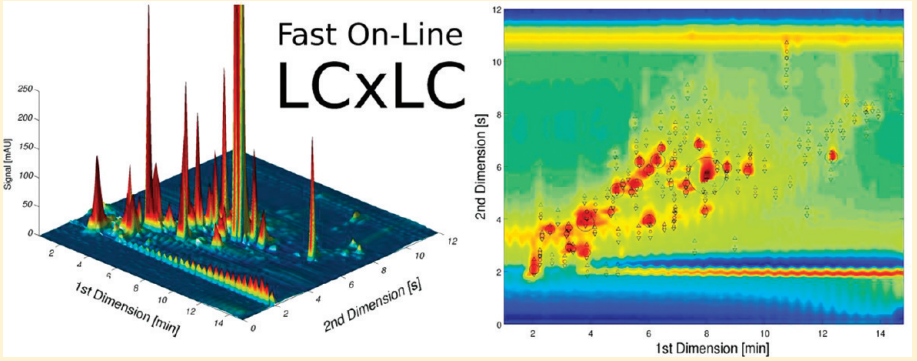

The use of flow splitters between the two dimensions in online comprehensive two-dimensional (2D) liquid chromatography (LC × LC) has not received very much attention, in comparison with their use in 2D gas chromatography (GC × GC), where they are quite common. In principle, splitting the flow after the first dimension column and performing online LC × LC on this constant fraction of the first dimension effluent should allow the two dimensions to be optimized almost independently. When there is no flow splitting, any change in the first-dimension flow rate has an immediate impact on the second dimension. With a flow splitter, one could, for example, double the flow rate into the first dimension column and perform a 1:1 flow split without changing the sample loop size or the sampler's collection time. Of course, the sensitivity would be diminished, but this can be partially compensated through the use of a larger injection; this will likely only amount to a small price to pay for this increased resolving power and system flexibility. Among other benefits, we found a 2-fold increase in the corrected 2D peak capacity and the number of observed peaks for a 15-min analysis time, using a post-first-dimension flow splitter. At a fixed analysis time, this improvement results primarily from an increase in the gradient time, resulting from the reduced system re-equilibration time, and, to a smaller extent, it is due to the increased peak capacity achieved by full optimization of the first dimension.

Since its introduction in 1991, the use of flow splitting as part of the modulator between the first and second dimensions in multidimensional gas chromatography has become quite common.[1] More recently, the various benefits of flow splitting have been discussed by Tranchida et al.[2] However, we have only seen a few references to the use of post-first-dimension flow splitting in online two-dimensional liquid chromatography (LC × LC);[3,4] flow splitting was not used for optimizing the first dimension in any of them. Block diagrams of online LC × LC systems without and with post-first-dimension flow splitting, as implemented in this work, are shown in Figures 1 a and 1 b, respectively.

In both systems, a comprehensive chromatogram is acquired; with use of a post-first-dimension flow splitter, only a fraction of the total effluent of the first dimension column is collected and delivered to the second dimension. This fraction is uniform and completely representative of the total effluent from the first dimension. This differs from the type of sampling described by Seeley,[3] where the duty cycle did not continuously collect the effluent coming from the first dimension; instead, discrete fractions were acquired at regular time periods.

The principal motivation for our interest in flow splitting in online LC × LC is best explained by our experiences in prior work. Previously, we and other researchers have shown that, in this form of LC × LC, there is necessarily an optimum sample acquisition time.[4,5] In online LC × LC, this sampling time (t_s) must be equal to the second dimension cycle time (^2t_c). Thus, the volume of sample collected when there is no

Received: September 1, 2011
Accepted: October 23, 2011
Published: October 23, 2011

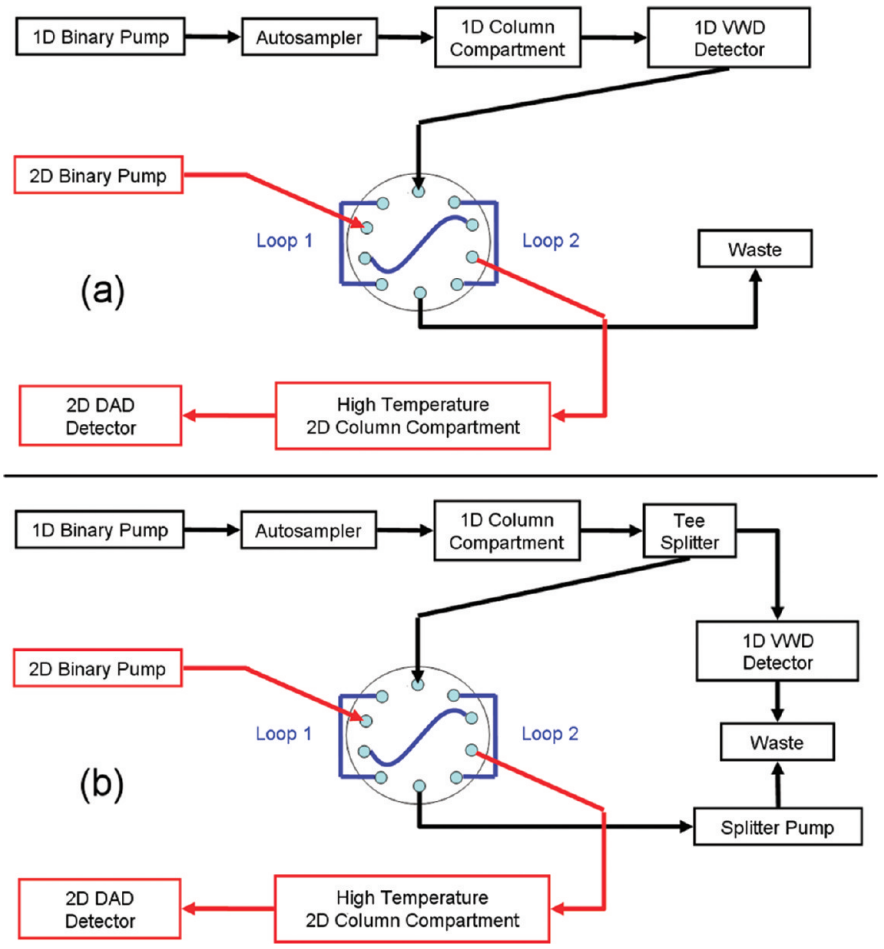

Figure 1. Block diagrams of the instruments used in the online two-dimensional liquid chromatography (LC × LC) separations for (a) split-less and (b) split modes.

splitter is given as

$$V_s = {}^1F \times {}^2t_c \quad (1)$$

It is evident that once the sampling time, which is equal to the second dimension cycle time, has been chosen, any change in the first dimension flow rate (${}^1F$) must result in a change in the sample volume with the split-less system shown in Figure 1 a. If a splitter were used as shown in Figure 1 b, eq 1 can be generalized to

$$V_s = \rho {}^1F \times {}^2t_c \quad (2)$$

where ρ is the "split ratio". Obviously, the smaller is the split ratio, the greater the dilution of the sample. This dilution effect in multidimensional separations has been studied by Schure[6] and, more recently, by Horvath et al.[7] The overwhelming chief virtue of this type of flow splitter is that it allows the two dimensions to be operated in an essentially independent manner. However, there are numerous other possible benefits, including, we believe, a significant enhancement in the resolving power of online LC × LC.

Giddings's peak capacity[8] has become the most important metric of separating power in multidimensional separations. It also has been shown, at least for one-dimensional liquid chromatography (1D-LC), that the peak capacity is proportional to the average resolution.[9] Ideally, the two-dimensional peak capacity ($n_{c,2D}$) is defined by the product of the peak capacities of the first dimension (${}^1n_c$) and that of the second dimension (${}^2n_c$) (the so-called "product rule"):

$$n_{c,2D} = {}^1n_c \times {}^2n_c \quad (3)$$

It is well-known that this equation overestimates the *practical* peak capacity of the system, and corrections must be applied to account for the undersampling of the first dimension[5,10,11] and for the lack of "orthogonality" of the separation mechanisms in the two dimensions.[12]

The product rule can be corrected for undersampling, using the Davis–Stoll–Carr factor:[11,13]

$$\langle\beta\rangle = \sqrt{1 + 3.35\left(\frac{{}^2t_c}{{}^1w}\right)^2} = \sqrt{1 + 3.35\left(\frac{{}^2t_c\,{}^1n_c}{{}^1t_g}\right)^2} \quad (4)$$

where β is the undersampling correction factor, ${}^1w$ the first dimension 4σ peak width, and ${}^1t_g$ the first dimension gradient time. By applying this correction factor to eq 3, we obtain the *corrected* 2D peak capacity ($n'_{c,2D}$):

$$n'_{c,2D} = \frac{{}^1n_c \times {}^2n_c}{\langle\beta\rangle} \approx \frac{{}^1t_g \times {}^2n_c}{{}^1w\sqrt{1 + 3.35\left({}^2t_c/{}^1w\right)^2}} \quad (5)$$

dx.doi.org/10.1021/ac202317m |*Anal. Chem.* 2011, 83, 9531–9539

Table 1. First-Dimension Operational Parameters and Peak Capacities for Various Analysis Times and Split Modes[a]

	Analysis Time = 15 min		Analysis Time = 30 min		Analysis Time = 60 min	
	split-less	split	split-less	split	split-less	split
gradient time, ${}^1t_g$ [min]	6	12.4	19	25	43	52.1
re-equilibration time, ${}^1t_{re\text{-}eq}$ [min]	9	2.6	11	5	17	7.9
${}^1\lambda$[b]	0.40	0.82	0.63	0.83	0.72	0.87
${}^1\lambda$ ratio[c]	2.05		1.31		1.20	
column length, ${}^1L$ [cm]	5	20	10	30	25	40
flow rate, ${}^1F$ [μL/min]	100	570	100	380	100	290
injection volume, $V_{injection}$ [μL]	1.5	8.57	1.5	5.7	1.5	4.35
injection delay [min]	4.9	0.86	4.9	1.29	4.9	1.69
initial eluent strength, ${}^1\phi_i$	0	0	0	0	0	0
final eluent strength, ${}^1\phi_f$	0.81	0.49	0.62	0.50	0.63	0.47
${}^1w_{ave}$ [s]	9.7	4.99	12.9	8.28	16.1	13.4
${}^1w_{ave}$ ratio[d]	1.94		1.55		1.20	
${}^1n_{c,pred}$[e]	46	228	94	275	149	317
${}^1n_{c,pred}$ ratio[f]	5.0		2.9		2.1	
${}^1n_{c,measured}$[g]	37	149	88	181	157	232
${}^1n_{c,measured}$ ratio[h]	4.0		2.1		1.5	

[a] Column is Zorbax SB-C3 2.1 mm i.d., 3.5 μm particles. Temperature is 40 °C. [b] Fraction of the analysis time devoted to the separation. [c] Ratio of ${}^1\lambda$ value for the split mode to that of the split-less mode. [d] Ratio of average peak width for split-less to split mode. [e] Predicted peak capacity obtained with the optimization procedure. [f] Ratio of predicted peak capacity for split to split-less mode. [g] Measured peak capacity calculated with eq 7, using average peak widths. [h] Ratio of measured peak capacity ratio for split to split-less mode.

We feel that the use of the corrected 2D peak capacity provides a more-accurate measure of the real resolving power and reasonably incorporates the effect of undersampling.

As online LC × LC becomes more widely adopted for quantitative analysis, replicate analyses and high throughput will become more important. In this respect, the analysis time must be as short as possible. The system re-equilibration time ($t_{re\text{-}eq}$) plays a key role in setting the gradient time (t_g) for a certain analysis time (t_{an}) and must be considered for optimization since no separation occurs during re-equilibration. The concept of the fraction of the analysis time devoted to the separation (λ) has been defined by Horvath et al. for the second dimension of a two-dimensional liquid chromatography (2D-LC) separation.[13,14] With the same objective in mind, we define its analogue for the first dimension of 2D-LC as

$$ {}^1\lambda = \frac{{}^1t_g}{{}^1t_{an}} = \frac{{}^1t_g}{{}^1t_g + {}^1t_{re-eq}} \quad (6) $$

This relationship will be used to represent the fraction of the analysis time that is devoted to the separation in the first dimension. Obviously, as the first dimension re-equilibration time occupies a smaller fraction of the total first-dimension analysis time, ${}^1\lambda$ approaches unity.

In this work, we will compare the time-based performance of the two system configurations (split and split-less), in terms of the corrected 2D peak capacity, as defined by eq 5. We also report the number of observed peaks in a complex maize extract sample as a complementary metric of the performance of the systems. These two metrics are very important, in that the instrumental configuration that yields the larger total corrected 2D peak capacity should also yield (for the same peak distribution) the larger number of observed peaks.[11] The corrected 2D peak capacity production rate is also calculated, because it is especially important in high-throughput analysis.

EXPERIMENTAL SECTION

Chemicals. The origin of most of the indolic standards used to determine the peak capacities has been described in previous work;[15] however, indole-5-carbonitrile, 4-indolyl acetate, as well as nitroethane and nitropropane, were purchased from Sigma−Aldrich (St. Louis, MO) as reagent-grade or better. Thiourea was reagent-grade, purchased from Matheson Coleman & Bell (East Rutherford, NJ, USA). Chromatographic-grade water and acetonitrile were obtained from Fisher Scientific (Pittsburgh, PA, USA). Perchloric acid (reagent-grade) was purchased from Sigma−Aldrich (St. Louis, MO, USA). All materials were used as received. All mobile phases were prepared gravimetrically (±0.01 g) and used without any further filtration.

Sample Preparation. Two samples were used in this experiment: a standard mixture and a maize extract. The standard mixture contained the following compounds: thiourea (33.9 μg/mL), 5-hydroxy-L-tryptophan (151 μg/mL), indole-3-acetyl-L-aspartic acid (27.1 μg/mL), indole-3-acetyl-L-glutamic acid (265 μg/mL), tryptophan (91.6 μg/mL), anthranilic acid (33.9 μg/mL), indole-3-acetyl-L-glycine (80.8 μg/mL), 5-hydroxy-tryptamin (22.9 μg/mL), indole-3-acetyl-ε-L-lycine (33.9 μg/mL), indole-3-acetyl-β-D-glucose (54.9 μg/mL) indole-3-acetamide (74.6 μg/mL), indole-3-carboxylic acid (91.6 μg/mL), indole-3-acetyl-L-isoleucine (61.8 μg/mL), indole-3-propionic acid (33.9 μg/mL), indole-3-ethanol (72.9 μg/mL), tryptamine (40.7 μg/mL), indole-3-butyric acid (133 μg/mL), indole-3-acetonitrile (102 μg/mL), indole-5-carbonitrile (48.5 μg/mL), 4-indolyl acetate (18.1 μg/mL), nitroethane (10.4 μg/mL), and nitropropane (9.9 μg/mL). The final solvent composition of the standard mixture was water with <1 vol % of acetonitrile. The maize seed used for the maize extract preparation was Silver Queen (Burpee, Warminster, PA), and a detailed procedure for its preparation has been given.[4] The samples were filtered through a 0.45-μm polytetrafluoroethylene (PTFE)

dx.doi.org/10.1021/ac202317m |Anal. Chem. 2011, 83, 9531–9539

membrane before injection, and the injected volumes are reported in Table 1.

It is most important to note that the injection volume for the standard mixture and maize extract samples were chosen to hold constant the number of moles of sample transferred from the first dimension to the second dimension. For example, at an analysis time of 15 min, using the split-less mode, the injection volume was 1.5 μL and the entire sample was transferred to the second dimension; the flow rate in the first dimension was fixed at 100 μL/min, delivering a sample volume of 20 and 34 μL for cycle times of 12 and 21 s, respectively. In the split mode, the first-dimension-optimized flow rate was 570 μL/min but the splitting pump was set to a flow rate of 100 μL/min. To compensate for the split flow, 8.57 μL (1.5 μL × 570/100) of sample were injected into the first dimension so that the same number of moles of sample would be delivered to the second dimension in both modes. This was done to ensure that peak counting was not affected by a change in sensitivity when the flow is split. In addition, in preliminary work (not shown), the amount injected was deliberately varied, to test for column overload. We are confident that the first dimension was not overloaded in either mode.

LC × LC Instrumentation—First Dimension. The system used an Agilent 1200 Model G1379 in-line micro vacuum degasser and an Agilent 1200 SL binary pump Model G1312, where the original mixer was replaced with a JetWeaver V100 mixer, also from Agilent. This allowed us to reduce both the flush-out volume to 700 μL and the delay volume of the system to 610 μL. This helps minimize the system flush-out time, which is part of the first-dimension re-equilibration time. The sample was introduced with an Agilent 1290 Infinity Autosampler Model G4226A equipped with a 40-μL loop cartridge. The chromatographic column was placed in an Agilent 1200 SL thermostatted column compartment Model G1312B. The detector used was an Agilent 1100 VWD Model G1314A, which was equipped with a 1-μL, 5-mm-path micro flow cell. When the system was configured in the split-less mode, the flow from the first dimension was fixed at 100 μL/min and all the effluent was collected after the detector, as shown in Figure 1a; when the system was configured in the split mode, the flow was divided into two streams, using a stainless steel "tee" (Model U-428, IDEX Corp., Lake Forest, IL, USA). One of the outputs was connected to the Agilent 1100 VWD UV detector Model G1314A equipped with a 1-μL, 5-mm-path micro flow cell, which then was connected to the waste line. The other output was connected to a 10-port/2-position valve (VICI CHEMINERT Model 110-0063H, Valco Instruments, Houston, TX, USA) for sampling the first dimension, as shown in Figure 1b. The flow path after the 10-port valve was connected to an Agilent 1290 Pump Model G4220A, which controls the flow of the incoming effluent at a flow rate of 100 μL/min. A 100 cm long × 0.0025 in. inner diameter (i.d.) of PEEK-Sil tubing was connected at the output of the pump, to provide sufficient backpressure for the check valves to operate properly. The 10-port valve was pneumatically actuated using helium at 80 psi. The two sample loops (loop 1 and loop 2 in Figure 1) were made of PEEK tubing: 37.5 cm long × 0.01 in. i.d. for a cycle time of 12 s and 137 cm long × 0.007 in. i.d. for a cycle time of 21 s. The volume of each set of loops is shown in Table 2.

The separation columns used for the first dimension were ZORBAX SB-C3 (2.1 mm i.d.) with 3.5 μm particles from Agilent, and columns 5, 10, 15, and 25 cm in length were connected to achieve the desired column length, according to the optimization protocol. Operational conditions used in both the split and split-less modes and peak capacities for the first dimensions are given in Table 1.

Table 2. Second-Dimension Operational Parameters and Peak Capacities[a]

	cycle time = 12 s	cycle time = 21 s
gradient time, ${}^2t_g$ [s]	9	18
re-equilibration time, ${}^2t_{re\text{-}eq}$ [s]	3	3
column length, ${}^2L$ [cm]	3.3	3.3
flow rate, ${}^2F$ [mL/min]	3.0	3.0
sample loop volume, V_{loop} [μL]	20	34
initial eluent strength, ${}^2\phi_i$	0	0
final eluent strength, ${}^2\phi_f$	1.0	1.0
${}^2n_{c,measured}$[b]	24	32

[a] Column is 3.3 cm long × 2.1 mm i.d. packed with ZirChrom-CARB 3 μm particles. Temperature is 110 °C. [b] Second-dimension peak capacity calculated by eq 8, using the measured average peak width.

LC × LC Instrumentation—Second Dimension. An Agilent 1290 binary pump Model G4220A configured with a JetWeaver Model V35 mixer was used in the second dimension of the online LC × LC system. The solvent in channel A was 10 mM aqueous phosphoric acid, and the solvent in channel B was acetonitrile. The second-dimension gradient time was either 9 or 18 s, with a fixed re-equilibration time of 3 s, regardless of the gradient time. The corresponding second-dimension cycle times were 12 and 21 s. An Agilent DAD detector Model G4220A was equipped with a 1-μL, 6-mm-path micro flow cell with a sampling rate of 80 Hz; data were acquired at a wavelength of 220 nm. The slit width was set to 4 nm and the reference wavelength set to "off".

The second-dimension separations were carried out on 2.1 cm × 33 mm columns packed in-house with 3.0 μm ZirChrom CARB particles (ZirChrom Separations, Inc., Anoka, MN, USA). The column was operated at 110 °C and a flow rate of 3.0 mL/min, corresponding to a maximum system pressure of ~400 bar during gradient elution. An eluent preheater and column heating system (Systec, Inc., New Brighton, MN, USA) was used to maintain the second-dimension column at 110 ± 0.1 °C. Columns with a small inner diameter (2.1 mm) were used to minimize thermal mismatch peak broadening.[16] The small dimensions of this column together with the high flow rate ensures a short system dwell time and fast column re-equilibration.[16,17] ZirChrom CARB was chosen as the second-dimension stationary phase for its good chemical and mechanical stability at high temperature and highly different selectivity relative to most RP stationary phases.[18] Operational conditions used for the second dimensions are in Table 2.

Data Acquisition and System Control. All Agilent modules were configured and controlled using Agilent Chemstation B.04.03-[16] (Agilent Technologies, Inc., USA). The binary pump used for the second dimension and the 10-port valve were coordinated by LabVIEW 9.0 software via a PCI 6024E data acquisition board (National Instruments, Inc., Austin, TX, USA), using a simple in-house program.

Data Processing. The data were acquired by the Chemstation software as a single run for each 2D experiment; the data were then exported as a comma-separated file and processed using Matlab 7.10 (R2010b, The Mathworks, Inc., Natick, MA, USA) with in-house programs.

Optimization and Calculation of Peak Capacities. A computational method for a priori optimization of gradient elution

peak capacity was developed by Wang et al.[9] This method maximizes the peak capacity through the prediction of gradient peak widths and retention times, based on the LSST theory.[19] For a given gradient time, column inner diameter, particle size, and maximum pressure available, the optimum column length, linear velocity, and final gradient composition are calculated to maximize the peak capacity. The indolic standard analytes were used to calibrate the optimization procedure. We believe that the indolic standard mixture is a good representative of the key components in the maize sample extract.[15] We followed this approach to optimize the first dimension for both the split and split-less modes. When the split-less mode is used, the flow rate was fixed at 100 μL/min, allowing only the column length and final gradient composition to be optimized. For the second dimension, we have experimentally shown[4] that an optimum sampling time exists. Accordingly, we decided to use two cycle times (12 and 21 s), which closely bracket the optimum for the current experiments.

We decided to use 2.1-mm columns for the first dimension in both modes. This was done because this column diameter works well at the sub-optimum flow rate of 100 μL/min needed in the split-less mode. In the split mode, we could have accommodated a larger-diameter (e.g., 4.6 mm) column. In order to make a conservative and simpler comparison of the two modes, we decided to keep the diameter constant. The use of a 4.6-mm-i.d. column in the split mode offers two advantages over the use of a 2.1-mm column. First, at the same linear velocity, the higher flow rate would diminish the system flush-out time, thereby increasing $^1\lambda$ even further (see below). Second, 4.6-mm-diameter columns generally offer more plates than 2.1-mm-diameter columns do.

Peak Capacity Measurement. The first-dimension peak capacity in optimized gradient conditions was measured using the indolic standard mixture. The peak capacity was calculated according to eq 7:

$$^1n_c = \frac{(t_{R,last} - t_{R,first})}{^1w_{avg}} \quad (7)$$

where $t_{R,last}$ and $t_{R,first}$ are, respectively, the retention times of the last and first peaks observed in the separation space and w_{avg} is the average 4σ peak width of all well-resolved peaks.

Because delayed injection was used in this work and the first peak in the samples always eluted near the column hold-up time, $t_{R,first}$ was taken as t_0. *A very important consideration is that the use of delayed injection also allows us to combine the time needed to flush the instrument dwell volume with part of the column flush-out/re-equilibration time*. Thus, for a long series of injections, we do not need to consider the instrument dwell. Through the use of delayed injection, the flushing of the system dwell is effectively combined with the re-equilibration of the column. For all these reasons, we believe that, in a fair comparison of the split and split-less modes, one should exclude the instrument dwell time, because that time is only paid once in a series of runs and is rapidly amortized. The operational conditions were optimized such that the last peak in our standard mixture eluted near the end of the gradient; $t_{R,last}$ was set equal to $t_0 + t_g$. The peak width in eq 7 was taken as the average 4σ peak width of all well-resolved compounds in the standard mixture.

The second-dimension peak capacity was calculated based on the average of the observed 4σ peak widths of representative well-formed second-dimension peaks in the online LC × LC separations of the maize extract. These second-dimension peaks were carefully chosen to avoid broad peaks caused by sample overloading, specific chemical interactions between the column and samples, and unresolved peaks. The peak capacity was then calculated according to

$$^2n_c = \frac{^2t_g}{^2w_{avg}} \quad (8)$$

In eq 8, ^2t_g is the second-dimension gradient time, which is $t_s - 3$ s in our experiments, and w_{avg} is the average 4σ peak width of the second-dimension separation.

The corrected 2D peak capacities at the specified first- and second-dimension gradient time combinations were calculated according to eq 5 and are reported in Table 3.

Table 3. Effect of Split Mode, Analysis Time, and Second-Dimension Cycle Time on Corrected 2D Peak Capacity and Corrected 2D Peak Capacity Production Rate

	Analysis Time = 15 min		Analysis Time = 30 min		Analysis Time = 60 min	
	split-less	split	split-less	split	split-less	split
(a) 12 s						
$^1n_{c,measured}$ [a]	37	149	88	181	157	232
$^2n_{c,measured}$ [b]	24	24	24	24	24	24
$\langle\beta\rangle$ [c]	2.5	4.5	2.0	2.8	1.7	1.9
$n'_{c,2D}$ [d]	360	793	1073	1534	2257	2912
$n'_{c,2D}/t_{an}$ [peaks/min] [e]	24	53	36	51	38	49
(b) 21 s						
$^1n_{c,measured}$ [a]	37	149	88	181	157	232
$^2n_{c,measured}$ [b]	32	32	32	32	32	32
$\langle\beta\rangle$ [c]	4.1	7.8	3.1	4.7	2.5	3.0
$n'_{c,2D}$ [d]	291	614	899	1221	1975	2456
$n'_{c,2D}/t_{an}$ [peaks/min] [e]	19	41	30	41	33	41

[a] First-dimension peak capacity calculated by eq 7, using the measured average peak width. [b] Second-dimension peak capacity calculated by eq 8, using the measured average peak. [c] First-dimension peak broadening factor, calculated by eq 4. [d] Corrected 2D peak capacity calculated by eq 5. [e] Corrected 2D peak capacity production rate, relative to analysis time.

Number of Peaks Observed in the Maize Extract. To confirm the trend in the results obtained with the corrected 2D peak capacity as a measure of the resolving power in 2D-LC, we counted the number of peaks observed in the maize extract. The procedure is based on a painstaking visual inspection of each individual second-dimension chromatogram and the manual merging of peaks that correspond to the same first-dimensional peak. This procedure has been described in detail.[4]

RESULTS AND DISCUSSION

2D-LC can be used either to generate very large peak capacities or to generate reasonably large peak capacities in a relatively short time.[20−22] While off-line LC × LC[23,24] is clearly the best way to generate very high peak capacities (but it is very expensive in terms of analysis time), online LC × LC is surely the best way to generate large peak capacities in a relatively short analysis time[21] (15−30 min). In both online and off-line modes, many restrictions apply, such as compatibility of mobile phases between both dimensions,[25,26] limits on volume of sample injected in the

dx.doi.org/10.1021/ac202317m |*Anal. Chem.* 2011, 83, 9531–9539

second dimension,[27] and the strength of the sampled solvent from the first dimension.[28,29]

In online LC × LC, another restriction applies, since the second-dimension analysis time must be equal to the sampling time (unless parallel columns are used), because the samples are sequentially analyzed in real time. This imposes a serious constraint, since both are tightly coupled. As a result, the peak capacity of each dimension is severely diminished. The second dimension must be very fast, to reduce the deleterious effect of undersampling the first dimension, but it must have an acceptable separating power (i.e., peak capacity). This also affects the first dimension, because flow rates much lower than optimum must be used to avoid injecting too large a sample volume into the second dimension. To reduce this effect, some researchers have used long capillary columns in the first dimension but still run them at flow rates lower than optimum.[27−31] With this strategy, both the instrument and column re-equilibration times are greatly increased.

Different approaches have been used to reduce this problem. Stoll et al. used a *pre-first-dimension flow splitter* with a split ratio of 10:1 to reduce the pumping system flush-out time.[22] The pump was working at a flow rate of 1000 μL/min, while the column received only 100 μL/min, which was also below its optimum flow rate. Occasionally, a post-first-dimension flow splitter was used to reduce the volume of sample collected in the loops without optimizing the flow rate, which was usually below the optimum.[10,32]

In those publications, where a post-first-dimension flow splitter was used the split ratio was invariably implemented by using a "tee" with the appropriate tubing lengths and inner diameters of the two branches chosen to create the desired relative flow resistances and, thus, the desired split ratio. We refer to this technique as *passive flow splitting*. In passive flow splitting, the split ratio under gradient conditions is affected by the viscosity of the fluid and thus is determined by the eluent composition and its temperature. Our approach is much less sensitive to fluctuations or differences in composition or temperature.

To the best of our knowledge, post-first-dimension flow splitting has never been used to maximize the peak capacity of the first dimension in online LC × LC. The novelty of this work is that the use of post-first-dimension flow splitting controlled by a metering pump has allowed us to fully optimize the first-dimension conditions independent of the second dimension and *precisely* control the split ratio. We refer to this as *active flow splitting*. Using active flow splitting, the split ratio is not affected by viscosity or temperature. It is important to note that, in the approach used here, the first-dimension separation is not affected by any change in the split ratio; in contrast, any change in the flow ratio of a pre-first-dimension flow splitter must alter the first dimension retention time. Using a pumping system to accurately control the flow rate of the branch that connects to the 10-port sampling valve allows accurate control of the sample introduced in the second dimension and the flexibility to change the split ratio as needed.

It has been shown that the first-dimension separation power is less important to the overall peak capacity than is the second dimension,[13,21,33] unless the gradient time is also increased. In this work, we predict and confirm an important improvement in the corrected 2D peak capacity, using post-first-dimension active flow splitting (see Tables 3 and 4).

Our calculations (see Table 1) using post-first-dimension column flow splitting predicted a 5-fold increase in the peak capacity of the first dimension (see data for an analysis time of 15 min) by fully optimizing not just the column length and final eluent composition, as was done in the split-less mode, but the use of the splitter also allows the optimization of the flow rate with its concomitant effect on column length and final effluent composition. The experimental results show a 4-fold increase in the observed first-dimension peak capacity (see Table 1). However, all of this gain is not actually realized in $n'_{c,2D}$, because such an increase in the first-dimension peak capacity (and, thus, a reduction in peak width in time units) is accompanied by an increase in the undersampling effect (see eq 5), as shown by Davis et al.[11]

Table 4. Effect of Analysis Time, Split Mode, and Second-Dimension Cycle Time on Corrected 2D Peak Capacity and Number of Observed Peaks

	Analysis Time = 15 min		Analysis Time = 30 min		Analysis Time = 60 min	
	split-less	split	split-less	split	split-less	split
(a) 12 s						
$n'_{c,2D}$ [a]	360	793	1073	1534	2257	2912
$n'_{c,2D}$ ratio [b]	2.20		1.43		1.29	
# observed peaks	36	113	111	158	165	213
# peaks ratio [c]	3.14		1.42		1.29	
(b) 21 s						
$n'_{c,2D}$ [a]	291	614	899	1221	1975	2456
$n'_{c,2D}$ ratio [b]	2.11		1.36		1.24	
# observed peaks	43	80	103	128	154	184
# peaks ratio [c]	1.86		1.24		1.19	

[a] Corrected 2D peak capacity calculated by eq 5. [b] Ratio of measured corrected 2D peak capacity for split to split-less mode. [c] Ratio of the number of observed peaks for split to split-less mode.

At longer analysis times (results shown for 30 and 60 min), the improvement is not as big as for the 15-min case. This is because, in both the split and split-less modes, the fraction of the time devoted to the gradient is larger, relative to the time spent re-equilibrating the system, as shown by $^1\lambda$ in Table 1. The peak capacity increases as $^1\lambda$ approaches unity. This effect can be easily observed in the chromatograms of the first dimension of the LC × LC experiments. In Figures 2a and 2b, the analysis time is 15 min and the time devoted for the separation is about half that for the split-less mode (see Table 1). As the analysis time was increased, the relative difference between the gradient and re-equilibration time became smaller but is still significant.

There are two factors that contribute to the increase in the first-dimension peak capacity shown in Table 1. First, the flow splitter allows a very significant increase in ^1t_g at the same analysis time (that is, an increase in $^1\lambda$). Second, the flow splitter allows us to work at a fully optimized flow rate, column length, and eluent composition. This results in a decreased average peak width (see Table 1).

A question arises: Which effect has the greater impact on the corrected 2D peak capacity? The question is not easily answered. Inspection of Table 1 shows that the $^1\lambda$ and ^1w ratios are approximately equal at all three analysis times, suggesting that both factors contribute equally to the improved corrected 2D peak capacity, *but this is misleading*.

Examination of eq 5 clearly shows that, when undersampling is fairly strong (that is, $\langle\beta\rangle$ is larger than unity (see Table 1)),

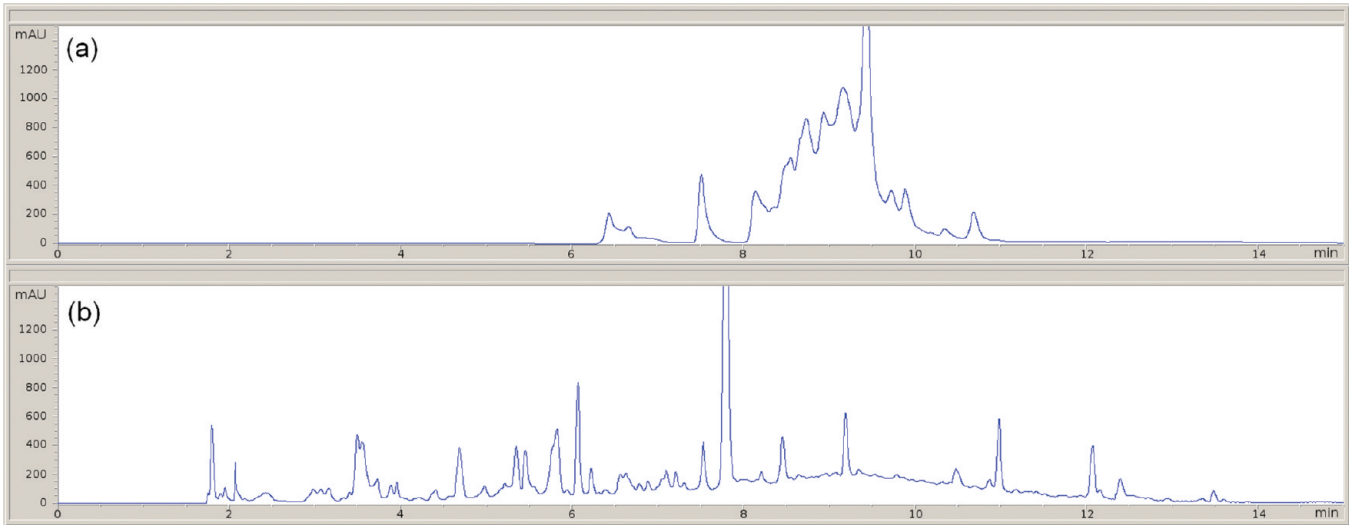

Figure 2. Chromatograms of the maize extract for an analysis time of 15 min, as acquired by the first-dimension detector for (a) split-less and (b) split modes. Experimental conditions were as described in Table 1.

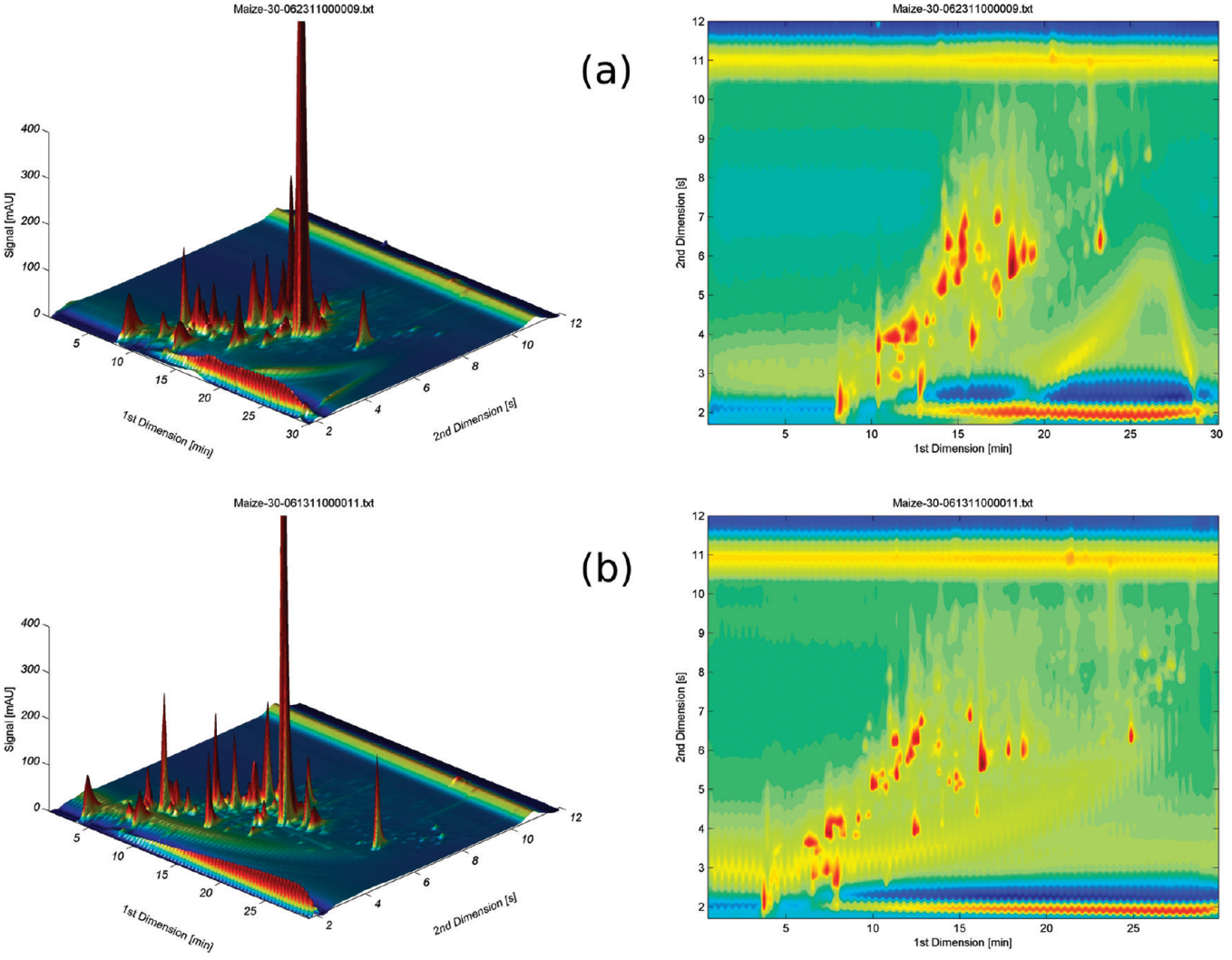

Figure 3. Three-dimensional (3D) and contour plots of the maize extract in (a) split-less mode and (b) split mode. Analysis time is 30 min, with a cycle time of 12 s.

dx.doi.org/10.1021/ac202317m |*Anal. Chem.* 2011, 83, 9531–9539

then a decrease in ${}^1w$ due to system optimization is almost canceled by the increase in the undersampling effect. The increase in $\langle\beta\rangle$ upon changing from the split-less mode to the split mode is quite large (see Table 3). Some simple computations using the form on the righthand side of eq 5 show that, at 15 min, the increase in the corrected 2D peak capacity, which is due solely to the increase in ${}^1t_g$ amounts to a factor of 2.07, whereas the increase due to only the decrease in ${}^1w$ is a factor of 1.07. The product of the two factors gives an increase of 2.20, in almost exact agreement with the observed increase in $n_{c,2D}$. Clearly, the dominant effect is the increase in ${}^1t_g$ and the concomitant improvement in ${}^1\lambda$.

It is also important to note (see Table 1) the lower final organic solvent composition in the gradient when the flow rate is optimized. This gives better focusing on the second dimension column. Another point, as shown in Table 4 at analysis times of <60 min, is that a cycle time of 12 s gives higher corrected 2D peak capacities and numbers of observed peaks than does a cycle time of 21 s. Actual 2D chromatograms are shown in Figure 3.

We chose to show results at an analysis time of 30 min because the rate of production of peak capacity is almost as high as at an analysis time of 15 min but the total peak capacity is significantly higher. It is evident, in both the 3D and contour plots of Figure 3, that the peaks are distributed over a wider range in first-dimension space in the runs with the flow splitter.

CONCLUSIONS

In this work, we have shown the benefits of using a post-first-dimension column active flow splitter to optimize the first-dimension conditions and improve the separation power in online LC × LC. The key conclusions are the following:

(1) The ability to optimize the first dimension independently from the second dimension allowed us to increase the corrected 2D peak capacity and the number of observed peaks by a factor of more than 2 at an analysis time of 15 min.
(2) This improvement is made possible primarily by reducing the system re-equilibration time, thus increasing the time allowed for the separation of the first dimension. A small secondary effect is the decrease in peak width that results from the optimization of the flow rate, column length, and final mobile phase composition.
(3) The flow splitter should allow the use of wider columns in the first dimension (e.g., 4.6 mm i.d.), which will result in even better usage of the time devoted to the separation in the first dimension increasing the overall separation power of online LC × LC.
(4) Using an active flow splitter gives the extra benefit of flexibility to control the amount of sample transferred into the second dimension *precisely*. This can be automated and adjusted as needed.
(5) Since the flow splitter is implemented after the first dimension column, the reproducibility of the separation in the first dimension is not affected by any change in the split ratio.

AUTHOR INFORMATION

Corresponding Author

*Tel.: (612) 624-0253. Fax: (612) 626-7541. E-mail: petecarr@umn.edu.

ACKNOWLEDGMENT

This work was financially supported by grants from the National Institutes of Health (NIH) (No. GM054585-15) and the National Science Foundation (NSF) (No. CHE-0911330). We also wish to acknowledge funding from the Agilent Foundation and the gifts of columns from Agilent Technologies, Inc. and ZirChrom Separations, Inc. M.F. wants to acknowledge a fellowship from ANPCyT-UNLP (Argentina). P.W.C. is deeply indebted to Leonid Blumberg for his advice and the gracious sharing of his profound knowledge of multidimensional chromatography.

REFERENCES

(1) Liu, Z.; Phillips, J. B. *J. Chromatogr. Sci.* **1991**, *29*, 227–231.
(2) Tranchida, P. Q.; Casilli, A.; Dugo, P.; Dugo, G.; Mondello, L. *Anal. Chem.* **2007**, *79*, 2266–2275.
(3) Seeley, J. V. *J. Chromatogr. A* **2002**, *962*, 21–27.
(4) Huang, Y.; Gu, H.; Filgueira, M.; Carr, P. W. *J. Chromatogr., A* **2011**, *1218*, 2984−2994.
(5) Horie, K.; Kimura, H.; Ikegami, T.; Iwatsuka, A.; Saad, N.; Fiehn, O.; Tanaka, N. *Anal. Chem.* **2007**, *79*, 3764–3770.
(6) Schure, M. R. *Anal. Chem.* **1999**, *71*, 1645–1657.
(7) Horvath, K.; Fairchild, J. N.; Guiochon, G. *J. Chromatogr. A* **2009**, *1216*, 7785–7792.
(8) Giddings, J. C. *Anal. Chem.* **1984**, *56*, 1258A–1260A, 1262A, 1264A.
(9) Wang, X.; Stoll, D. R.; Schellinger, A. P.; Carr, P. W. *Anal. Chem.* **2006**, *78*, 3406–3416.
(10) Murphy, R. E.; Schure, M. R.; Foley, J. P. *Anal. Chem.* **1998**, *70*, 1585–1594.
(11) Davis, J. M.; Stoll, D., R.; Carr, P. W. *Anal. Chem.* **2007**, *80*, 461–473.
(12) Schure, M. R. In *Multidimensional Liquid Chromatography: Theory, Instrumentation and Applications*; Cohen, S. A., Schure, M. R., Eds.; Wiley & Sons: New York, 2008.
(13) Potts, L. W.; Stoll, D. R.; Li, X.; Carr, P. W. *J. Chromatogr., A* **2010**, *1217*, 5700–5709.
(14) Horvath, K.; Fairchild, J. N.; Guiochon, G. *Anal. Chem.* **2009**, *81*, 3879–3888.
(15) Stoll, D. R.; Cohen, J. D.; Carr, P. W. *J. Chromatogr. A* **2006**, *1122*, 123–137.
(16) Thompson, J. D.; Brown, J. S.; Carr, P. W. *Anal. Chem.* **2001**, *73*, 3340–3347.
(17) Snyder, L. R.; Glajch, J. L.; Kirkland, J. J. *Practical HPLC Method Development*, 2nd ed.; Wiley & Sons: New York, 1996.
(18) Gu, H.; Huang, Y.; Filgueira, M.; Carr, P. W. *J. Chromatogr. A* **2011**, *1218*, 6675−6687.
(19) Snyder, L. R.; Dolan, J. W. *High-Performance Gradient Elution: The Practical Application of the Linear-Solvent-Strength Model*; Wiley & Sons: Hoboken, NJ, 2007.
(20) Horváth, K.; Fairchild, J.; Guiochon, G. *J. Chromatogr. A* **2009**, *1216*, 2511–2518.
(21) Guiochon, G.; Marchetti, N.; Mriziq, K.; Shalliker, R. A. *J. Chromatogr. A* **2008**, *1189*, 109–168.
(22) Stoll, D. R.; Li, X.; Wang, X.; Porter, S. E. G.; Rutan, S. C.; Carr, P. W. *J. Chromatogr., A* **2007**, *1168*, 3–43.
(23) Marchetti, N.; Fairchild, J. N.; Guiochon, G. *Anal. Chem.* **2008**, *80*, 2756–2767.
(24) Eeltink, S.; Dolman, S.; Ursem, M.; Swart, R.; McLeod, F.; Schoenmakers, P. J. *LCGC Europe* **2009**, *22*, 404.
(25) Wei, Y.; Lan, T.; Tang, T.; Zhang, L.; Wang, F.; Li, T.; Du, Y.; Zhang, W. *J. Chromatogr., A* **2009**, *1216*, 7466–7471.
(26) Dugo, P.; Favoino, O.; Luppino, R.; Dugo, G.; Mondello, L. *Anal. Chem.* **2004**, *76*, 2525–2530.
(27) Vivo-Truyols, G.; van der Wal, S.; Schoenmakers, P. J. *Anal. Chem.* **2010**, *82*, 8525–8536.

(28) Jandera, P.; Hájek, T.; Cesla, P. *J. Chromatogr. A* **2011**, *1218*, 1995–2006.
(29) Groskreutz, S. R.; Swenson, M. M.; Secor, L. B.; Stoll, D. R. *J. Chromatogr. A*, in press (DOI: 10.1016/j.chroma.2011.06.035).
(30) Francois, I.; de Villiers, A.; Tienpont, B.; David, F.; Sandra, P. *J. Chromatogr. A* **2008**, *1178*, 33–42.
(31) Cacciola, F.; Delmonte, P.; Jaworska, K.; Dugo, P.; Mondello, L.; Rader, J. I. *J. Chromatogr. A* **2011**, *1218*, 2012−2018.
(32) Macnair, J. E.; Lewis, K. C.; Jorgenson, J. W. *Anal. Chem.* **1997**, *69*, 983–989.
(33) Li, X.; Stoll, D. R.; Carr, P. W. *Anal. Chem.* **2008**, *81*, 845–850.